Available online at www.sciencedirect.com
ScienceDirect
Journal of Computational Physics 227 (2008) 9271–9291
JOURNAL OF COMPUTATIONAL PHYSICS
www.elsevier.com/locate/jcp

LES approach for high Reynolds number wall-bounded flows with application to turbulent channel flow

C. Pantano [a,*], D.I. Pullin [b], P.E. Dimotakis [b], G. Matheou [b]

[a] *Department of Mechanical Science and Engineering, University of Illinois at Urbana-Champaign, 1206 W. Green Street, Urbana, IL 61801, USA*
[b] *Graduate Aeronautical Laboratories, California Institute of Technology, MC 105-50, 1200 E. California Blvd., Pasadena, CA 91125, USA*

Received 18 April 2007; received in revised form 18 February 2008; accepted 8 April 2008
Available online 26 April 2008

Abstract

We describe a large-eddy simulation approach for turbulent channel flow using the stretched-vortex subgrid-scale model. The inner region of the turbulent boundary layer is not included in the modeling of this attached, wall-bounded flow. Appropriate boundary conditions and closure are derived using a combination of elements from asymptotic expansions, matching, and well-established wall-modeling approaches. The modeling approach for this application combines the stretched-vortex subgrid model with a localized wall-shear-stress treatment that relates the instantaneous wall-parallel velocity to the shear stress via the log-law, as appropriate for this (near-) zero pressure gradient flow. The impermeability boundary condition is built into the method such that only the outer-flow solution is simulated, obviating the need to impose the stiff no-slip condition at the wall. This formulation attempts to minimize numerical and modeling errors introduced by the boundary-condition treatment, while preserving the fundamental elements required to predict low-order statistics of these flows. We present simulation results for turbulent channel flow up to Reynolds number based on the wall-friction velocity of 10^6. These compare favorably with results from large-scale DNS and experimental correlations.

Keywords: LES; Numerical methods; Turbulence modeling; Wall functions; Law of the wall; Boundary conditions

1. Introduction

The structure of the turbulent boundary layer can be described roughly in terms of two regions: an inner region, where viscous effects dominate and whose thickness scales on wall-friction variables, and an outer region, where more-classical turbulent transport may be assumed. Direct numerical simulation (DNS) of the large range of scales spanned by the ensuing dynamics is impractical at the high Reynolds numbers of interest in many applications. For this reason, large-eddy simulation (LES) is pursued as an alternative. Most

* Corresponding author. Tel.: +1 217 244 1412.
E-mail address: cpantano@uiuc.edu (C. Pantano).

0021-9991/$ - see front matter © 2008 Elsevier Inc. All rights reserved.
doi:10.1016/j.jcp.2008.04.015

LES numerical modeling of wall-bounded turbulent flows is hampered by the absence of large-scale eddies adjacent to the inner region [1,2]. Ideally, one would like to perform LES of the outer boundary-layer and interior-flow regions, while accommodating inner-region physics via an appropriate boundary treatment [3]. Currently, such flows present severe physical and numerical-modeling challenges, particularly in engineering codes that are largely only second-order accurate and use relatively coarse mesh resolution. These challenges represent some of the outstanding issues in wall-bounded turbulence modeling.

The most successful LES techniques today rely on a "partially resolved" approach in which the no-slip boundary condition is used without a wall model. The filter size, or more appropriately the cutoff scale, decreases as one approaches the wall to permit resolution of an acceptable fraction of the energy within the near-wall eddies. Very skewed grids are typically required in such simulations at practical Reynolds numbers, with wall-parallel directions captured in high-aspect-ratio cells with a much coarser streamwise extent to reduce computational cost. An important limitation of this approach is that computational cost scales approximately as the square of the friction Reynolds number [4], rendering its application to most practical flows infeasible.

The additional resolution in the wall-normal direction is necessary to resolve the high gradients resulting from the no-slip boundary condition. Even so, the physics of the inner layer must still be neglected since the grid cannot represent it in the wall-parallel directions. Some savings can be achieved using an adaptive-mesh refinement strategy to decrease the computational cost [5]. If these computational costs are to be minimized, the inner region that is adjacent to the wall must be appropriately modeled.

The main challenge that must be addressed is presented by the no-slip wall boundary condition that is felt in three ways: (1) by removing mass flux near the wall, albeit a decreasing amount with increasing Reynolds number; (2) by imposing a wall shear stress that is transported and must be represented in the simulation of the outer boundary-layer and interior regions of the flow [3]; (3) by local heating, attendant entropy production, and energy transport, even though the latter is important only in high-speed, wall-bounded flows that are not considered here. If in simulating the outer boundary-layer and interior flows the no-slip condition is not explicitly incorporated, its consequences must be, in the sense of an inner/outer asymptotic expansion, here implemented numerically. That requires the correct inner–outer matching condition to be imposed, in view of Items 1 and 2, above, as well as Item 3 for high-speed-flow simulations [6] that is not part of the focus of this paper, however.

A simulation of the outer boundary-layer and interior flow regions that does not include the no-slip condition and the (in-the-limit) singular region that results from it must be informed of the consequences of the missing dynamics. In the proposed approach and for the flow at hand, this is achieved using the zero pressure gradient (ZPG) Law-of-the-Wall [7] as a boundary condition that conveys the required wall shear-stress information as a necessarily independent input to the simulation scheme.

The quality of the simulation results using this approach depends strongly on controlling the coupling between the physical model and the numerical approximations. This requires understanding of the complicated specific interaction between the subgrid closure and the numerical implementation of the (effective) boundary conditions at the wall [8].

The importance of the subgrid scale model has been highlighted (e.g., [9]) although it appears that the most important source of variability of LES results lies in the wall treatment itself [10]. A widely used method has been to use the dynamic Smagorinsky subgrid closure together with a wall shear-stress model, also called a wall function, as documented in a number of specific models [11].

A first wall model that can be viewed as providing an approximate boundary condition was introduced by Deardorff [12] who constrained the wall-normal derivatives of the wall-parallel velocity to recover the logarithmic law, on average. This was followed by Schumann [3], who first used a wall function relating the instantaneous velocity in the first cell off-wall to the total shear stress, thereby enforcing the correct momentum flux. A large number of methods and refinements have been proposed to obtain the functional dependence of the wall function on available fields of the LES [13–21]. An alternative approach is to use a zonal model in which an auxiliary, very fine mesh is used next to the wall to solve a boundary-layer type equation and resolve the no-slip boundary condition. Reynolds-averaged Navier–Stokes (RANS) or simplified wall laws derived from these equations and complemented by blending functions to diminish the contribution from the eddy viscosity near the wall are used here, with a dynamic Smagorinsky model (e.g., [22–26]). Yet another approach, called detached-eddy simulation (DES), does not require explicit blending functions, solving, instead, a transport equation for the turbulent kinetic energy close to the wall and blending with the LES in the resolved flow

region [27]. Approaches that include generalizations of the dynamic Smagorinsky subgrid-scale model that is made aware of the scale non-invariance as the wall is approached have also been developed [28], as well as formulations that include more-detailed stochastic effects [29–31]. Some work has been carried out to incorporate anisotropic effects and backscatter in the subgrid closure itself [32–34], whose importance is recognized at the wall. While results obtained with these techniques may be satisfactory at low or moderate Reynolds numbers in complex geometries and even moderately high Reynolds number in simple geometries, there remains a need for improved mathematical and modeling to enable robust LES for general flows at the high Reynolds numbers of practical interest. In this respect, and for a method to be sufficiently general, the subgrid closure must inevitably be formulated using a parameterization with localized support, i.e., no averaging along the wall-parallel directions or any other global operator. Additionally, the numerical implementation details and the discretization errors must be carefully considered.

There exist variations in technique, mostly using the dynamic Smagorinsky model, that involve a number of modeling parameters whose physical justification is still a matter of research. Nevertheless, available references suggest that important deficiencies in these models remain when average statistics are compared with expected inner scalings of these flows.

It could be argued that the idea of Schumann [3] is physically reasonable and one would expect this closure to be satisfactory, provided the physical dynamics are correctly represented in the simulations and Reynolds number and numerical issues, including grid cell size next to the wall, are correctly implemented. As Cabot and Moin [11] note, it is now largely accepted that the majority of the deficiencies with wall-function treatments for coarse resolution LES lie in both the numerical approximations used to represent the strain tensor with low-order (one-sided) differences next to the boundary and in the inaccuracies of the physical subgrid model itself when applied in the vicinity of the wall. Therefore, implementation details of both the numerical and subgrid models are central to this type of flow modeling.

The discussion above suggests that there are two main approaches to tackling the wall-closure problem. In one approach, research is concentrated in understanding why the simple, but physically based, wall shear-stress closures perform only marginally well, while other research avenues investigate more complex wall closures. This paper reports results of the former approach, using the particular but important example of channel flow at high Reynolds numbers as an illustration.

The discussion describes a formulation that attempts to minimize *ad hoc* modeling and numerical choices by considering near-wall modeling from the point of view of a simulation of outer boundary-layer and interior flow scales only. This requires the specification of a proper boundary condition that is compatible with the flow and, at the same time, conveys the correct average physics to the resolved flow scales. In this context, the subgrid-scale model close to the wall must act as if there is no wall present, behaving mostly as in the free shear-flow regions of the outer-boundary layer and interior of the domain. This is achieved by an appropriate extension of the velocity field that effectively continues the flow seen by the subgrid model below the wall. The major advantage of this formulation is that no *ad hoc* blending functions or numerical parameters are required and the quality of the statistical results is high over a range of Reynolds numbers.

2. Mathematical formulation

We consider a domain of size L_m in the x_m directions with $m = 1, 2, 3$, respectively. The streamwise direction is x_1, the wall-normal coordinate x_2 and the spanwise direction x_3. The Favre-filtered form of the Navier–Stokes (momentum) equations is used to simulate the flow,

$$\frac{\partial \bar{\rho}\tilde{u}_l}{\partial t} + \frac{\partial(\bar{\rho}\tilde{u}_l\tilde{u}_m + \bar{p}\delta_{lm} - \bar{\sigma}_{lm} + \tau_{lm})}{\partial x_m} = \bar{\rho}\tilde{f}_l, \tag{1}$$

together with the mass- and energy-conservation equations,

$$\frac{\partial \bar{\rho}}{\partial t} + \frac{\partial \bar{\rho}\tilde{u}_m}{\partial x_m} = 0, \tag{2}$$

$$\frac{\partial \overline{E}}{\partial t} + \frac{\partial((\overline{E} + \bar{p})\tilde{u}_m + \bar{q}_m - \bar{\sigma}_{mq}\tilde{u}_q + q_m^{\mathrm{T}})}{\partial x_m} = \bar{\rho}\tilde{f}_q\tilde{u}_q, \tag{3}$$

where repeated indices denote summation, t, is time, and resolved quantities are given by $\bar{\rho}$ for density, $\tilde{u}_l$ the velocity components, $\bar{p}$ the pressure, $\bar{\sigma}_{lm}$ the Newtonian stress tensor, $\overline{E}$ total energy, $\bar{q}_m$ the heat flux, and $\tilde{f}_l$ the body force. Overbars denote Reynolds-averaged quantities, given for an arbitrary field ϕ by,

$$\bar{\phi}(x_m,t) = \int_{-\infty}^{\infty} G(x_m - x'_m)\phi(x'_m,t)\,\mathrm{d}x'_m, \tag{4}$$

where G denotes the filter kernel and it is understood that the integral is a three-dimensional convolution in space. Tilde denotes Favre-averaged quantities given by $\tilde{\phi} = \overline{\rho\phi}/\bar{\rho}$. There is no distinction between Favre and conventionally filtered quantities for incompressible constant-density flow. In some occasions, we will refer to $\tilde{u}_1, \tilde{u}_2, \tilde{u}_3$ as $\tilde{u}, \tilde{v}, \tilde{w}$, respectively, and $x_1 = x, x_2 = y, x_3 = z$ to simplify the notation. The subgrid terms that need to be modeled are the subgrid-stress tensor and the subgrid heat flux,

$$\tau_{lm} = \bar{\rho}(\widetilde{u_l u_m} - \tilde{u}_l\tilde{u}_m), \tag{5}$$

$$q_m^{\mathrm{T}} = \bar{\rho}(\widetilde{c_p T u_m} - \tilde{c_p}\widetilde{T}\tilde{u}_m), \tag{6}$$

respectively, where c_p denotes the specific heat of the mixture at constant pressure and $\widetilde{T}$ the temperature. State and constitutive relations are given by,

$$\overline{E} = \frac{\bar{p}}{(\gamma-1)} + \frac{1}{2}\bar{\rho}(\tilde{u}_l\tilde{u}_l) + \frac{1}{2}\tau_{ll}, \tag{7}$$

$$\bar{\sigma}_{lm} = \bar{\mu}\left(\frac{\partial\tilde{u}_l}{\partial x_m} + \frac{\partial\tilde{u}_m}{\partial x_l} - \frac{2}{3}\delta_{lm}\frac{\partial\tilde{u}_q}{\partial x_q}\right), \tag{8}$$

$$\bar{q}_m = -\bar{\lambda}\frac{\partial\overline{T}}{\partial x_m}, \tag{9}$$

where γ is the ratio of specific heats and $\bar{\mu}$ and $\bar{\lambda}$ denote the filtered dynamic viscosity and heat conduction coefficients, respectively. The filtered pressure, $\bar{p}$, is determined from the ideal equation of state $\bar{p} = \bar{\rho}R\widetilde{T}$, where R is the ideal-gas constant for the fluid. Since our subgrid model provides the complete subgrid-stress tensor, $\bar{p}$ is the actual resolved pressure field. This approach differs from the incompressible formulation using the Smagorinsky subgrid closure, for example, where the non-deviatoric part of the subgrid-stress tensor is lumped together with the pressure.

For compactness of notation, we define the vector of conservative state variables, $\{\overline{Q}_l\} = \{\bar{\rho}\tilde{u}, \bar{\rho}\tilde{v}, \bar{\rho}\tilde{w}, \bar{\rho}, \overline{E}\}$, for the resolved momentum, mass, and total energy. Similarly, the second term appearing in the left-hand side of Eqs. (1)–(3), generally referred-to as the flux tensor, is defined as,

$$F_{lm} = \begin{cases} \rho u_l u_m + p\delta_{lm} - \sigma_{lm} & l \leqslant 3, \\ \rho u_m & l = 4, \\ (E+p)u_m + q_m - \sigma_{mq}u_q & l = 5. \end{cases} \tag{10}$$

The corresponding filtered counterpart, $\overline{F}_{lm}$, is obtained by applying Eqs. (4)–(10). This last operation leads to the subgrid-closure problem.

2.1. Boundary conditions

In a 'resolved' LES simulation, the customary no-slip boundary condition is imposed at the wall, i.e.,

$$\tilde{u} = \tilde{v} = \tilde{w} = 0. \tag{11}$$

In the modeling approach adopted here, where only outer boundary-layer and interior scales of the wall-bounded flow are simulated, this boundary condition, Eq. (11), is replaced by an alternative set of boundary conditions that is compatible with the dynamics captured in the simulation of the resolved-flow regions. This set of boundary conditions must be consistent with the numerical implementation and, dynamically, have a small impact on the quality of the first- and second-order statistics prediction. The original idea of Schumann [3] offers a boundary closure choice. In this approach for a non-transpiring boundary, the total momentum flux tangential to the wall is specified in the form of,

$$\overline{F}_{\alpha m} n_m = \tau_{w,\alpha}(\bar{\rho}, \tilde{u}_i, \Delta x_m, \mu, \text{ surface properties}), \tag{12}$$

where the Greek letter α denotes wall-parallel directions ($\alpha = 1, 3$ in our case) and n_m is the normal to the surface pointing in the direction outwards of the fluid domain. In this expression, the function $\tau_{w,\alpha}$ represents a closure, here algebraic, that depends parametrically, in principle, on all available (resolved) fields.

The derivation of these boundary conditions uses Eq. (4) and integration by parts of the Navier–Stokes equations to derive Eq. (1). The conceptual filter operator, G, introduced in Eq. (4) only from a formal point of view, must now have compact support. This implies that the resolved (filtered) equations remain well-defined only to a certain minimum distance off the wall, from the point of view of the large turbulent scales.

We will not dwell on several theoretical extensions available in the literature that accommodate for the complexities that arise if the filter kernel is allowed to intersect the wall. In our case, this minimum distance controls the location of the first grid-node off the wall. The present development assumes a filter function, G, that is a top-hat filter kernel, given by,

$$G(x_m - x'_m) = \frac{1}{\Delta V} \begin{cases} 1 & \text{for } |x_m - x'_m| \leqslant \frac{\Delta x_m}{2}, \\ 0 & \text{otherwise}, \end{cases} \tag{13}$$

where $\Delta V = \Delta x_1 \Delta x_2 \Delta x_3$. The filtered momentum equation, Eq. (1), evaluated at $x_2 = \Delta x_2/2$ from the wall, can be rewritten in the equivalent form,

$$\frac{\partial}{\partial t}\frac{1}{\Delta V}\int_{\Delta V} \rho u_l \, \mathrm{d}\Omega + \frac{1}{\Delta V}\int_{\Delta V} \frac{\partial}{\partial x_m}(\rho u_l u_m + p\delta_{lm} - \sigma_{lm})\, \mathrm{d}\Omega = \bar{\rho}\tilde{f}_l, \tag{14}$$

where $\mathrm{d}\Omega = \mathrm{d}x_1\, \mathrm{d}x_2\, \mathrm{d}x_3$. The element ΔV is now decomposed into $\Delta V_O \bigcup \Delta V_I$ (see Fig. 1) where the height of the thin volume ΔV_I is $\delta x_2 \ll \Delta x_2$. For near-wall modeling, we require that the majority of flow features associated with near-wall structures are contained within ΔV_I. Utilizing Gauss's theorem on V_O and V_I for the wall-parallel momentum components, u_α, the second term in the left-hand side of Eq. (14) can now be approximated and rewritten in divergence form,

$$\begin{aligned} &\int_{\Delta V} \frac{\partial}{\partial x_m}(\rho u_\alpha u_m + p\delta_{\alpha m} - \sigma_{\alpha m})\, \mathrm{d}\Omega \\ &\quad \approx \int_{\Delta V_O} \frac{\partial}{\partial x_m}(\rho u_\alpha u_m + p\delta_{\alpha m} - \sigma_{\alpha m})\, \mathrm{d}\Omega \\ &\quad = \int_{\Delta S_O} (\rho u_\alpha u_m + p\delta_{\alpha m} - \sigma_{\alpha m}) n_m \, \mathrm{d}S \\ &\quad = (\overline{F}^{O^+}_{\alpha 1} - \overline{F}^{O^-}_{\alpha 1})(\Delta x_2 - \delta x_2)\Delta x_3 + (\overline{F}^{O^+}_{\alpha 2} - \overline{F}^{O^-}_{\alpha 2})\Delta x_1 \Delta x_3 + (\overline{F}^{O^+}_{\alpha 3} - \overline{F}^{O^-}_{\alpha 3})\Delta x_1 (\Delta x_2 - \delta x_2), \end{aligned} \tag{15}$$

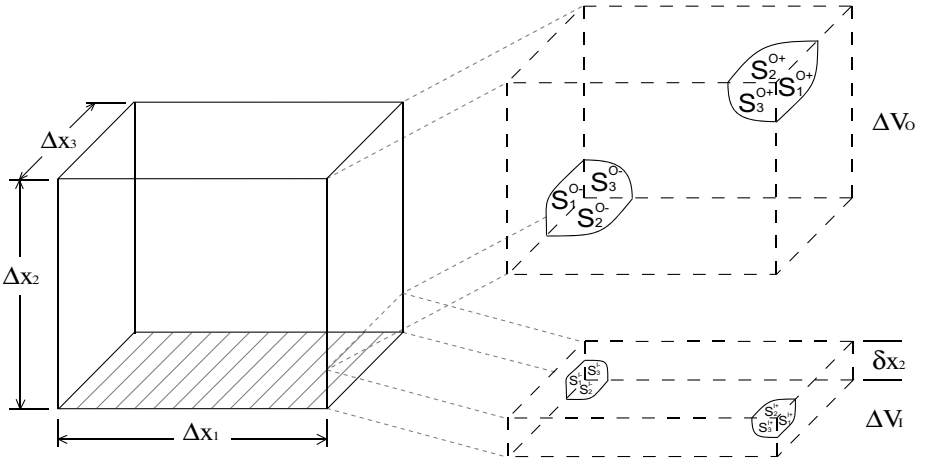

Fig. 1. Sketch of a grid cell next to the wall.

where we have used the notation $\overline{F}^{\mathrm{O}^{\pm}}_{\alpha n}$ to denote the surface-averaged values of $F_{\alpha n}$ at the bottom/left/back (−) or top/right/front (+) surfaces $S_n^{\mathrm{O}^{\pm}}$ of the control volume ΔV_{O} normal to direction n,

$$\overline{F}^{\mathrm{O}^{\pm}}_{\alpha,n} = \frac{\Delta x_n}{\Delta V}\int_{S_n^{\mathrm{O}^{\pm}}} F_{\alpha,n}\,\mathrm{d}S. \tag{16}$$

Applying the same approach to the average momentum equation in the ΔV_{I} volume, gives,

$$\frac{\partial}{\partial t}\int_{\Delta V_{\mathrm{I}}} \rho u_\alpha\,\mathrm{d}\Omega + (\overline{F}^{\mathrm{I}^+}_{\alpha 1} - \overline{F}^{\mathrm{I}^-}_{\alpha 1})\delta x_2\Delta x_3 + (\overline{F}^{\mathrm{I}^+}_{\alpha 2} - \overline{F}^{\mathrm{I}^-}_{\alpha 2})\Delta x_1\Delta x_3 + (\overline{F}^{\mathrm{I}^+}_{\alpha 3} - \overline{F}^{\mathrm{I}^-}_{\alpha 3})\Delta x_1\delta x_2 = \Delta V_{\mathrm{I}}\bar{\rho}\tilde{f}_\alpha. \tag{17}$$

This equation can be rewritten to express $\overline{F}^{\mathrm{I}^+}_{\alpha 2}$ as a function of the other terms, i.e.,

$$\overline{F}^{\mathrm{I}^+}_{\alpha 2} = \overline{F}^{\mathrm{I}^-}_{\alpha 2} + \delta x_2\bar{\rho}\tilde{f}_\alpha - \frac{1}{\Delta x_1\Delta x_3}\frac{\partial}{\partial t}\int_{\Delta V_{\mathrm{I}}}\rho u_\alpha\,\mathrm{d}\Omega - (\overline{F}^{\mathrm{I}^+}_{\alpha 1} - \overline{F}^{\mathrm{I}^-}_{\alpha 1})\frac{\delta x_2}{\Delta x_1} - (\overline{F}^{\mathrm{I}^+}_{\alpha 3} - \overline{F}^{\mathrm{I}^-}_{\alpha 3})\frac{\delta x_2}{\Delta x_3}. \tag{18}$$

The so-called equilibrium assumption neglects all terms but the first on the right-hand side and yields,

$$\overline{F}^{\mathrm{O}^-}_{\alpha 2} \equiv \overline{F}^{\mathrm{I}^+}_{\alpha 2} \approx \overline{F}^{\mathrm{I}^-}_{\alpha 2} = -\tau_{\mathrm{w},\alpha}. \tag{19}$$

These are nonlinear boundary conditions since $\overline{F}_{\alpha,n}$ and $\tau_{\mathrm{w},\alpha}$ cannot be expressed as linear combinations of the resolved velocity and its gradients. In our case, these two boundary conditions are,

$$(\bar{\rho}\tilde{u}_\alpha\tilde{u}_2 - \bar{\sigma}_{\alpha 2} + \tau_{\alpha 2}) = \pm\tau_{\mathrm{w},\alpha}, \tag{20}$$

when evaluated at the walls, $y = \pm h$.

The first underlying feature of Eq. (19) or Eq. (20) is to assume an instantaneous correlation between the available fields and the shear stress, without any temporal lag, as appropriate to the low Mach number flow under consideration here. This may be justified for computational grids of hundreds or even thousands of inner units at high Reynolds numbers, since the filter or average volume implied by the LES is sufficiently large that fluctuations do not contribute systematic errors in the mean velocity profiles. The second underlying assumption is to neglect the actual thickness of the inner zone, which occupies a small sub-volume of the first grid cell, with respect to the volume of the outer zone in the first grid cell next to the wall. This can be justified because the ratio of these two scales becomes vanishingly small at the high Reynolds numbers of interest. The third assumption is to neglect small temporal scales at the wall. These temporal scales are filtered out, both by the boundary-condition model and by the time step taken by the numerical method that is controlled by the resolved, outer-region of the flow.

2.2. Subgrid-scale model

The stretched-vortex subgrid-scale model, originally developed for incompressible LES [35] and extended to compressible flows [36], is used to provide estimates of the stress tensor, τ_{im}, and turbulent heat flux, q_m^{T}. In this model, the flow within a computational grid cell is assumed to result from an ensemble of straight, nearly axisymmetric vortices aligned with the local resolved strain rate tensor. This model is based on subgrid elements in the form of spiral vortices that are local approximate solutions of the exact Navier–Stokes equations [37]. The resulting subgrid stresses and energy flux are [36],

$$\tau_{lm} = \bar{\rho}\tilde{k}(\delta_{lm} - e_l^v e_m^v), \tag{21}$$

$$q_m^T = -\bar{\rho}\frac{\triangle_{\mathrm{c}}}{2}\tilde{k}^{1/2}(\delta_{ml} - e_m^v e_l^v)\frac{\partial(\tilde{c}_p\widetilde{T})}{\partial x_l}, \tag{22}$$

where $\tilde{k} = \int_{k_{\mathrm{c}}}^{\infty} E(k)\,\mathrm{d}k$ is the subgrid energy, $\boldsymbol{e}^{\boldsymbol{v}} = \{e_l^v\}$ is the unit vector aligned with the subgrid vortex axis and $k_{\mathrm{c}} = \pi/\triangle_{\mathrm{c}}$ represents the largest resolved wavenumber with $\triangle_{\mathrm{c}}$ the subgrid cutoff scale. The subgrid turbulent kinetic energy, $\tilde{k}$, is estimated by assuming a spiral vortex [37], whose Kolmogorov-like energy spectrum for the subgrid motion is given by,

$$E(k) = K_0\epsilon^{2/3}k^{-5/3}\exp[-2k^2\nu/(3|\tilde{a}|)], \tag{23}$$

where K_0 is the Kolmogorov prefactor, ϵ is the local cell-averaged dissipation (resolved flow plus subgrid scale), ν is the kinematic viscosity taken as $\tilde{\mu}/\bar{\rho}$, and $\tilde{a} = \widetilde{S}_{lm} e_l^v e_m^v$ is the axial strain along the subgrid vortex axis, where

$$\widetilde{S}_{lm} = \frac{1}{2}\left(\frac{\partial \tilde{u}_l}{\partial x_m} + \frac{\partial \tilde{u}_m}{\partial x_l}\right), \tag{24}$$

denotes the resolved rate-of-strain tensor. The subgrid vortex is presumed to be aligned, e_l^v, in the direction of the principal extensional eigenvector of $\widetilde{S}_{lm}$. This ansatz has been shown to work well in free-shear flows [38].

To close the model, the group prefactor, $K_0\epsilon^{2/3}$, must be calculated for each cell from the resolved flow. This is obtained by a structure–function matching [38–40], where the second-order velocity structure function, $\mathcal{F}_2(r)$ with separation r, when averaged over the surface of a sphere of radius $\triangle$, gives

$$\overline{\mathcal{F}_2}(\triangle) = \frac{4}{\triangle}\int_0^{\pi} E(s/\triangle)\left(1 - \frac{\sin s}{s}\right) \mathrm{d}s. \tag{25}$$

The spectra, Eq. (23), and the assumption that the exponential can be ignored when evaluating at the separation scale $\triangle$, give the group prefactor,

$$K_0\epsilon^{2/3} = \frac{\overline{\mathcal{F}_2}(\triangle)}{\triangle^{2/3} A}, \tag{26}$$

where $A = 4\int_0^{\pi} s^{-5/3}(1 - s^{-1}\sin s)\,\mathrm{d}s \approx 1.90695$. Frequently, $\triangle$ and $\triangle_c$ are taken to be the average grid spacing, $(\Delta x_1 \Delta x_2 \Delta x_3)^{1/3}$, as in the present simulations, and the spherical average of the structure function is computed as a local estimate using a six-point stencil of the resolved velocity components,

$$\overline{\mathcal{F}_2}(\triangle) = \frac{1}{6}\sum_{l=1}^{3}\sum_{m=1}^{3}(\delta^2 \tilde{u}_l)_m, \tag{27}$$

where $(\delta^2 \tilde{u}_l)_m = (\tilde{u}_l(\boldsymbol{x} + e_m \Delta x_m) - \tilde{u}_l(\boldsymbol{x}))^2 + (\tilde{u}_l(\boldsymbol{x} - e_m \Delta x_m) - \tilde{u}_l(\boldsymbol{x}))^2$ denotes the square of the lth velocity component difference in the Cartesian direction e_m (not related to the subgrid vortex alignment direction $\boldsymbol{e}^v$) at the point $\boldsymbol{x} = \{x_1, x_2, x_3\}$ [38].

2.3. Wall-function model

For a statistically homogeneous and stationary flow in the wall-parallel directions, an ensemble-averaged quantity is defined by,

$$\overline{\phi}(y) = \int_{-\infty}^{\infty} \Phi \mathcal{P}(\Phi; y)\,\mathrm{d}\Phi, \tag{28}$$

where $\mathcal{P}$ denotes the probability-density function of ϕ at location y and Φ denotes the state-space variable associated with ϕ. The wall function represents the relationship that is observed, experimentally, between the independent wall-normal coordinate and the ensemble-averaged wall-parallel velocity. This relationship is generally expressed in terms of inner variables,

$$y^+ = \frac{y u_\tau}{\nu}, \tag{29}$$

in the form called the "Law-of-the-Wall" and given by,

$$u^+ = f(y^+), \tag{30}$$

where $u^+ = \overline{\tilde{u}}/u_\tau$ is the inner-scaled ensemble-averaged velocity with friction velocity $u_\tau = \sqrt{\overline{\tilde{\tau}}_w/\bar{\rho}_w}$ and where the subscript 'w' denotes wall values. To render the discussion less cumbersome in this section, the y coordinate is measured starting at zero in the normal direction to each wall and increasing towards the inside of the flow domain.

For simplicity, we assume a two-layer model with Millikan's zero pressure gradient (ZPG) logarithmic law of the wall, whose origin goes back to Prandtl, which parameterizes the average velocity profile and has the form,

$$f(y^+) = \begin{cases} \frac{1}{\kappa}\ln(y^+) + B, & \text{if } y^+ > y^*, \\ y^+, & \text{if } y^+ \leqslant y^*. \end{cases} \tag{31}$$

In the proposed implementation it is assumed that this relationship holds instantaneously at each cell next to the wall. The value of y^* is the matching point of the two profiles, i.e.,

$$\frac{1}{\kappa}\ln(y^*) + B = y^*.$$

The von Kármán constant, κ, and the slope intercept, B, are accepted here with the values of 0.4 and 5, respectively. Some variation of these constants is reported in the literature but we have accepted these values as representative [41,42].

The main difficulty with Eq. (30) is that $\overline{\tau}_w$ is not known *a priori*. The wall-function closure approach assumes $\overline{\tau}_w = \tau_w$ and inverts Eq. (30) for a specific value of y^+ and $\overline{u}$ to recover u_τ, according to,

$$u_\tau = \overline{u} g\left(\frac{y\overline{u}}{\nu}\right). \tag{32}$$

where g is obtained by inverting Eq. (30) with a specific choice of f given by Eq. (31). Once u_τ is known, the shear stress, τ_w, can be expressed as,

$$\tau_w = \mathrm{sign}(\overline{u}) \times \bar{\rho}_w(|\overline{u}| g(y|\overline{u}|/\nu))^2, \tag{33}$$

such that the relationship is valid for both positive and negative $\overline{u}$. We note that the dependence of $\overline{u}$ on y should be such that, ideally, the value of τ_w that is inferred using resolved-flow information near the wall should be independent of y, for small y; certainly if the Law-of-the-Wall is to be obeyed.

Alternatively, one may use the model of Nickels [43], for example, to estimate the effect of the small but finite pressure gradient in the channel flow with a smooth wall, which closely osculates the classical ZPG parameterization but extends to non-ZPG boundary layers. Defining the non-dimensional pressure-gradient parameter, $p_x^+ = (\nu/\rho_w u_\tau^3)\,\mathrm{d}P/\mathrm{d}x$, and using the known pressure gradient for a periodic channel flow that is related to the shear stress through $\bar{\rho}\tilde{f}_1 = -\mathrm{d}P/\mathrm{d}x = \tau_w/h$, gives,

$$p_x^+ = -\frac{1}{Re_\tau}. \tag{34}$$

This is negligible in the high Reynolds number simulations we discuss here, according to the criteria proposed by Nickels [43], indicating that the ZPG Law-of-the-Wall should be more than adequate for the flow simulated.

3. Discretization

A collocated finite-difference discretization is employed where all variables are defined at the center of the computational cells. The nodal coordinates are equally spaced by $\Delta x_m = L_m/N_m$, where N_m is the number of grid points in the corresponding direction. The variable arrangement is such that all fields are collocated at the center of the grid cells. Thus, for a physical wall located at $y = x_2 = -h$, the center of the first off-wall cell is $x_2 = \Delta x_2/2 - h$. This arrangement is similar to that of the wall-parallel velocity components in staggered meshes and some wall-shifted discretizations of channel flow [44], while the wall-normal velocity is arranged differently in these alternative discretizations.

A finite-difference solver suitable for the simulation of the compressible LES equations is used to perform the present simulations [45]. In order to minimize interference of the numerical truncation error with the LES subgrid-scale model [46], a second-order-accurate, 5-point-wide stencil is used that is optimized in wavenumber space for LES [47]. This solver uses skew-symmetric derivative operators and third-order Runge–Kutta time integration. No explicit filters of any type are used in this formulation. Furthermore, while the equations

solved are for compressible flow, we selected a Mach number that is sufficiently low to minimize compressibility effects [6]. All test simulations correspond to a pressure-driven turbulent channel flow with a channel centerline mean Mach number of 0.15 and an adiabatic wall boundary condition for the energy equation.

Eqs. (2) and (3) are discretized in space at grid locations, $x_i = \Delta x(i-1/2)$, $y_j = \Delta y(j-1/2) - h$, and $z_k = \Delta z(k-1/2)$ where i, j, k denote indices varying from 1 to N_1, N_2 and N_3, respectively. Therefore, a field with a spatial dependence $\phi(x,y,z)$ is approximated at the locations $\phi(i,j,k) = \phi(x_i, y_j, z_k)$ (temporal dependence omitted for clarity).

Rewriting the finite-difference equations in terms of the fluxes of mass, momentum, and energy, we have,

$$\frac{\partial \overline{Q}_l}{\partial t} = -\frac{\Delta \overline{F}_{lm}}{\Delta x_m} + \bar{\rho}\tilde{f}_l. \tag{35}$$

Boundary conditions are prescribed according to the discussion in Section 2.1 to close the system of Eqs. (2) and (3) at the walls. Periodic boundary conditions in the x and z direction are used.

For the purposes of illustration of the approach described in this paper, the specific choice of the finite-difference stencil, such as order of accuracy and stencil width, does not play a role in the derivation of the boundary condition and subgrid closure at the wall. These will influence convergence rates and the minimum number of points required to resolve the flow structures, but will not affect the numerical issues associated with the physical closure of the inner zone described in this paper. Manipulation of the discrete equations in the form of Eq. (35) plays a crucial role in the treatment, as will be shown, however, and is not in accord with typical practice. Finite-volume discretizations lead most naturally to this form of the equations, but when using finite differences further operations must be performed to recover the flux form. It is sufficient to use the flux form only for those cells next to the wall; all other cells can be handled in the standard differential form.

3.1. Wall-function evaluation

The required terms in Eq. (20), $\tau_{w,1}$ and $\tau_{w,3}$, are now closed by assuming that, for high Reynolds number flow, the first cell in the computational domain extends well within the logarithmic-law region, e.g., $y^+ > 30$. In these conditions, the Law-of-the-Wall is assumed to hold approximately locally and instantaneously through a functional relationship,

$$\tau_{w,1} = \mathrm{sign}(\overline{\tilde{u}}^\dagger) \times \bar{\rho}_w(|\overline{\tilde{u}}^\dagger| g(y^\dagger|\overline{\tilde{u}}^\dagger|/\nu))^2, \tag{36}$$

$$\tau_{w,3} = \mathrm{sign}(\overline{\tilde{w}}^\dagger) \times \bar{\rho}_w(|\overline{\tilde{w}}^\dagger| g(y^\dagger|\overline{\tilde{w}}^\dagger|/\nu))^2, \tag{37}$$

where

$$\overline{\tilde{u}}^\dagger \approx \tilde{u}(x, y^\dagger, z, t), \tag{38}$$

$$\overline{\tilde{w}}^\dagger \approx \tilde{w}(x, y^\dagger, z, t). \tag{39}$$

The coordinate $y^\dagger$ denotes the location where the wall function is evaluated to recover the shear stress at the wall. In our case, we chose $y^\dagger = \Delta y/2$. This is a split-type wall model, where each wall-parallel direction is treated independently. It is also possible to implement a non-split model in which the coordinates are first rotated to be aligned with the wall-parallel velocity direction [48]. No measurable difference was observed using this approach, likely because $\tilde{u} \gg |\tilde{w}|$ for the Reynolds number and grid sizes considered here. The results reported are only with the split technique.

Instantaneous wall functions have been used previously [11] and result in what is also called the equilibrium stress-balance model in the context of turbulent boundary-layer modeling. The implementation described here departs from previous work in the manner in which the boundary condition is applied and coupled with the subgrid scale model according to Eqs. (41)–(43).

As will be shown, the closure of Eq. (31) plays an important role. We deliberately avoid a more-complex expression for f that could accommodate and represent the requisite physics with an improved parameterization and increased fidelity to illustrate the methodology and to limit the number of free parameters of the model. Only well-known and understood properties of the turbulent boundary layer at (near) zero pressure gradient are used in the flow simulated. In particular, while a suitably blended functional form for f could

be used, inner–outer matching is designed to occur in the logarithmic region and the inner (viscous) layer is only included to accommodate possible instantaneous fluctuations that may dip into the linear viscous regime. It is certainly possible and desirable, if not necessary in general circumstances [16], to improve on Eq. (31) by including complex geometrical effects as occur in recirculation zones [49], pressure-gradient effects [43] extending to flow separation, wall roughness, and even the stochastic variability between near-wall velocity and shear stress [30,31]. Such parameterizations, however, are unnecessary to simulate the flow at hand and not employed here. This point is discussed further below.

3.2. Discrete boundary conditions

To minimize compounding of numerical and modeling errors, the boundary conditions, Eqs. (36) and (37), must be enforced directly as part of Eq. (35) to ensure discrete momentum conservation in the mean. For this reason, the flux form of the governing equations is important. Use of Eq. (20) as a boundary condition for the LES implies, effectively, that the average momentum transfer from the inner region is applied to the outer resolved scales of the LES. This traction-type boundary condition is mathematically well-posed [50] and replaces two no-slip boundary conditions for $\tilde{u}$ and $\tilde{w}$ appearing in Eq. (11). Consideration of mass conservation within the first computational cell in contact with the wall shows that, to leading order, we must retain the no-penetration boundary condition, $\tilde{v} = 0$, in the wall-normal direction to enforce global mass conservation.

Some care is required when evaluating $\overline{F}_{12}(i, 3/2, k)$ and $\overline{F}_{32}(i, 3/2, k)$. Fig. 1 shows a sketch of the grid arrangement next to the wall. For a split numerical method where each direction is treated independently, the horizontal fluxes can be determined with no difficulty. On the other hand, the vertical flux at $x_2 = \Delta x_2$, S_2^{O+}, must be determined paying special attention to the dependent variables involved. In fact, for a second-order centered stencil, the momentum flux $\overline{F}_{12}(i, 3/2, k)$, contains a contribution from the subgrid stresses calculated at the center of the first cell, that is,

$$\overline{F}_{12}(i, 3/2, k) = \text{regular convective flux part} + \frac{1}{2}[\tau_{12}(i, 1, k) + \tau_{12}(i, 2, k)]. \tag{40}$$

However, calculation of $\tau_{12}(i, 1, k)$ requires knowledge of $\tilde{u}_i$ below the wall surface, or different formulas to Eqs. (24) and (27) to be used to determine all the quantities required in the subgrid model. We refer here to the methodology for extending the stencils used in the subgrid model to determine the subgrid stresses next to the wall (biased stencils). The issue arises for any subgrid model that involves gradients. The primary concern is the determination of the subgrid stresses τ_{ij} at these grid cells, using information that is consistent and compatible with the differential equation and the boundary conditions. The method implemented extrapolates the velocity field outside of the flow domain in halo or ghost cells below the wall. This extrapolated field is used to determine the subgrid stresses only and not any other terms of the discretized governing equations. For the lower wall of the channel, the extrapolations are,

$$\tilde{u}(i, 1 + n, k) = \tilde{u}(i, 1, k) + n\Delta x_2(\tilde{u}(i, 2, k) - \tilde{u}(i, 1, k)), \tag{41}$$

$$\tilde{v}(i, 1 + n, k) = -\tilde{v}(i, -n, k), \tag{42}$$

$$\tilde{w}(i, 1 + n, k) = \tilde{w}(i, 1, k) + n\Delta x_2(\tilde{w}(i, 2, k) - \tilde{w}(i, 1, k)), \tag{43}$$

where $n = -1, -2, \ldots$. The extrapolations implement the no-penetration boundary condition by reversing (reflecting) the vertical velocity component. It may be advantageous to use higher-order extrapolation, instead of linear (first-order) extrapolation, although this has not been pursued because the present numerical method employed is only second-order accurate (away from boundaries). The use of halo or ghost cells, $j \leqslant 0$, is not mandatory, and one can implement the extrapolation formulas directly as part of the subgrid model when approaching the wall. We note that no additional boundary data are contained in Eqs. (41)–(43), given that the extrapolation relies only on boundary data already imposed, along with information on computational cells inside the domain, derived from the LES equations themselves. Therefore, the extrapolation does not represent an additional boundary condition, according to the theory of partial differential equations (e.g., [51]).

An important characteristic of the present approach is that no damping functions are required to gradually reduce the magnitude of the subgrid stresses as the wall is approached. This has been shown to be necessary

with the constant-coefficient Smagorinsky model, for example, if first-order statistics are to be recovered [52,11]. Damping functions are not generally used with the dynamic Smagorinsky model in so-called "resolved" LES or even in simulations at moderately high Reynolds numbers that do not resolve the viscous subrange [53]. Nevertheless, some treatment of the eddy viscosity close to the wall appears necessary in coarse simulations of high Reynolds number channel flow [20].

4. Simulation results

The performance of the new boundary formulation and subgrid model is tested in a pressure-gradient driven turbulent channel flow configuration. The dimensions of the computational domain for all cases are $L_1 = 8\pi h$, $L_3 = 3\pi h$, where h is the channel half height. The grid is uniform in each direction and no adaptive mesh refinement is employed. Table 1 lists the number of points used in the uniform grids of the LES in all directions, the friction-based Reynolds number,

$$Re_\tau \equiv \frac{u_\tau h}{\nu} \tag{44}$$

and the value of κ used for the wall-function boundary condition, Eq. (31). For comparison, we have matched the parameters of the recent DNS of Hoyas and Jiménez [54] at $Re_\tau = 2003$ in case A2K (bulk Reynolds number 87,180). The non-uniform DNS grid relies on a total of $N_{\mathrm{DNS}} = 1.79 \times 10^{10}$ grid points (cf. Table 1) and clustering is used close to the walls to improve resolution and reduce computational cost.

Table 2 lists some statistics obtained from the simulations, with angle brackets denoting wall-parallel planar averages. The first column denotes the average value of the location of the first point above the wall in wall coordinates. The second column lists the standard deviation of y_1^+, denoted as $\sigma_{y_1^+}$. The third column denotes the ratio of volume-averaged subgrid kinetic energy,

$$K_{\mathrm{sgs}} = \frac{1}{2h}\int_{-h}^{h} \langle \tilde{k} \rangle \, \mathrm{d}y,$$

to the total volume-averaged kinetic energy, K, for each case. The last column denotes the normalized error between the value of the logarithmic-law intercept constant, B, in Eq. (31) and the value measured from the simulations, B_{sim}, where

$$E_B = \frac{B_{\mathrm{sim}} - B}{B}. \tag{45}$$

The error in the intercept constant is always negative with some statistical variability. It is unclear if this is a result of the coarse resolution or the limited domain size used. Nevertheless, the maximum error in B is of the

Table 1
Parameters of the DNS [54] and the present LES simulations

	N_1	N_2	N_3	$N_{\mathrm{total}} = N_1 N_2 N_3$	Re_τ	κ
DNS	6144	633	4608	1.79×10^{10}	2003	–
A2K	578	46	216	5.74×10^{6}	2003	0.4
B20K	800	64	302	1.54×10^{7}	2×10^{4}	0.4
B100K	800	64	302	1.54×10^{7}	10^{5}	0.4
B1M	800	64	302	1.54×10^{7}	10^{6}	0.4

Table 2
Averaged quantities from LES simulations

	$\langle y_1^+ \rangle$	$\sigma_{y_1^+}$	K_{sgs}/K	E_B
A2K	41.73	3.16	0.170	~0
B20K	312.5	17.47	0.166	−0.120
B100K	1562	71.52	0.209	−0.098
B1M	15,625	540.1	0.213	−0.123

order of 12%, a number that is small considered the large values of $\langle y^+ \rangle$ considered here. It may be argued that performing the inner–outer matching at such high values of the scaled y coordinate, $y^+_{\text{match}} = y^\dagger$, would be expected to incur systematic error with increasing $y^\dagger$. Certainly, one could employ the Coles's [55] Law-of-the-Wall/Law-of-the-Wake parameterization to address this concern. This was not attempted here because it would introduce an additional parameter and, as can be seen in Table 2, the small error in B does not exhibit a systematic increase with increasing $y^\dagger$.

We discuss the first case, A2K, and the comparisons with the DNS, since this constitutes our validation run. Fig. 2 shows a comparison of the average streamwise velocity for case A2K and the DNS result. As can be seen, even with as few as 23 points across the half channel height, the results are satisfactory. The first point in the computational mesh is, on average, at $y_1^+ \approx 42$. Even the few points next to the wall agree well with the DNS result, with a total mass flux error of only 1.7%. Fig. 3 shows comparisons of the subgrid and total velocity intensities in the three directions as well as of the shear-stress profiles. As can be seen, at this level of resolution with significant subgrid contributions, the agreement between DNS and LES is good. The effect of the wall model is limited to the first cell next to the wall, as commonly found in this type of modeling [53]. This is to some extent to be expected, since the boundary modeling only contains information about average stresses at the wall and no fluctuation model is provided. Fig. 3 shows a relative peak odd-grid oscillations of 3.4%, with respect to the mean stress profile, in the first few cells next to the wall on the total normal, spanwise and shear-stress profiles. It is not clear at this time why these small oscillations arise or what would be required to remove them, or if it is possible to eliminate them from the simulations within the modeling approach pursued here. This issue is postponed to the next section where we discuss some general limitations of the wall-function modeling approach employed.

Next, we increase the friction Reynolds number while keeping the number of points in the simulation constant. Fig. 4 shows comparisons of LES results for the average streamwise velocity with increasing friction Reynolds numbers, up to $Re_\tau = 10^6$. All cases collapse reasonably well when plotted in inner coordinates, despite the increasing scaled coarseness of the simulations and the extremely high Reynolds numbers. No parameters are modified, apart from the Reynolds number, to perform these simulations. Close inspection of the average velocity profiles seems to indicate what appears as a undershoot of the velocity profiles in the lower y^+ region of each simulation. More careful investigation shows that this is a display artifact that is a consequence of the slightly lower logarithmic-law intercept recovered from the simulations and reported in the last column of Table 2.

Another feature of the subgrid closure is that it leads to the development a wake region, with no other input, as a consequence of the coupling between the inner-scale modeling employed and the turbulence in the resolved flow, even at rather coarse resolutions. This feature is not usually observed in coarse LES simulations using the dynamic Smagorinsky model with wall-function closure, for example [11]. The wake part of

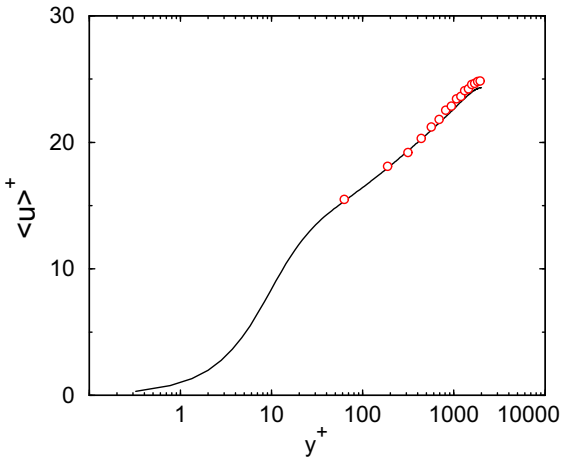

Fig. 2. Comparison of the mean streamwise velocity of the LES (symbols) with DNS (line) at $Re_\tau = 2003$.

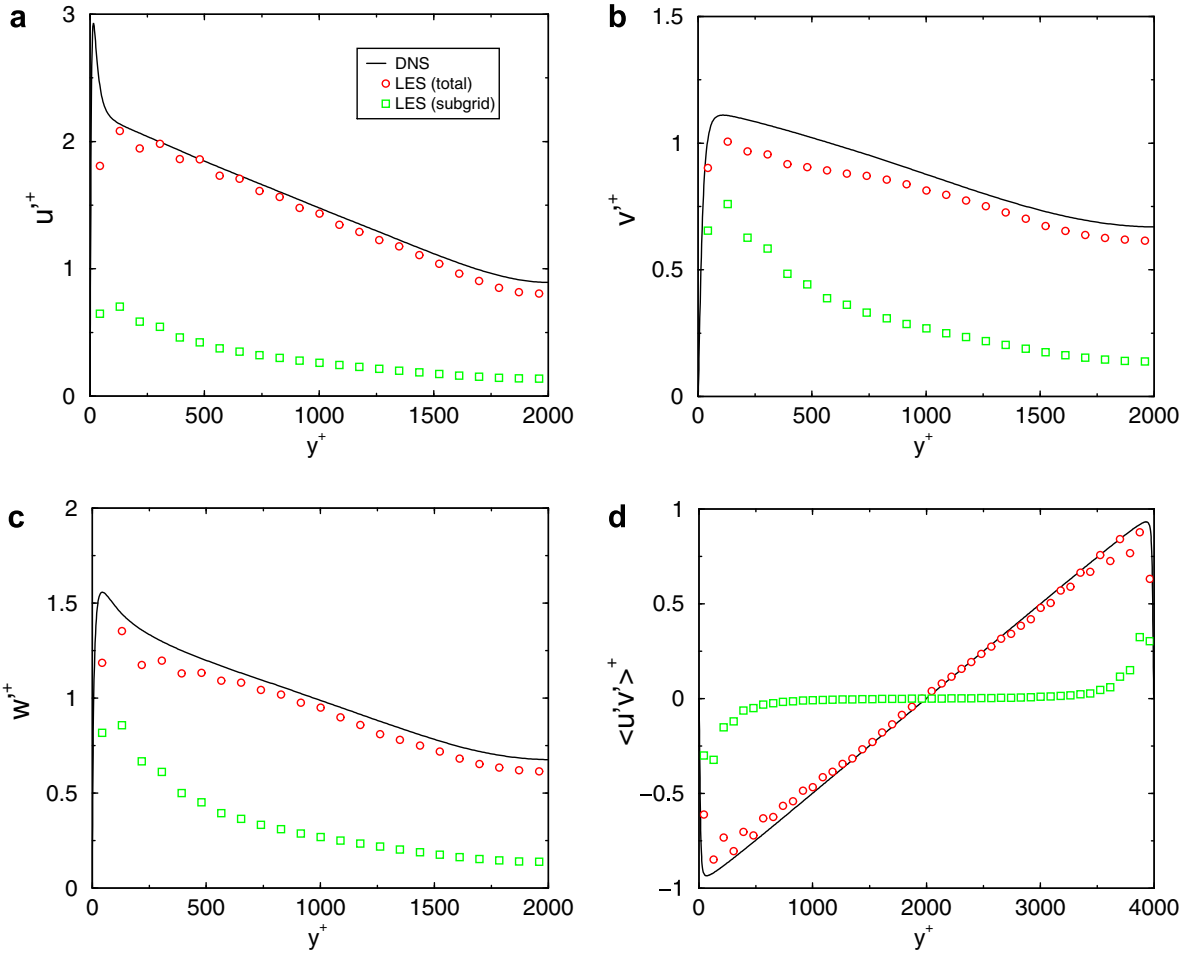

Fig. 3. Comparison of turbulent intensities from LES with DNS results: (a) streamwise intensity; (b) vertical intensity; (c) spanwise intensity; (d) shear stress.

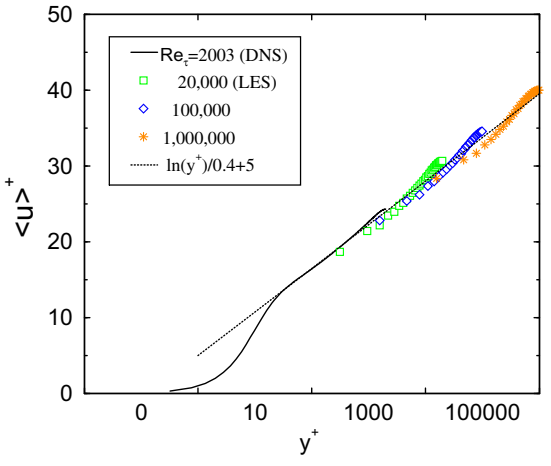

Fig. 4. Effect of Reynolds number on the average streamwise velocity for simulation series B.

the profiles suggests a wake magnitude, i.e., a departure from the logarithmic law at the center of the channel, of approximately one unit. This is well within the literature scatter for this quantity [56].

A second important derived quantity is the friction coefficient. This is defined as $C_f = 2(u_\tau/U_b)^2$, where U_b is the average bulk-flow velocity defined as

$$U_b = \frac{1}{V}\int_V \tilde{u}\,d\Omega. \tag{46}$$

C_f is a fundamental quantity that LES should predict.

Fig. 5 shows the friction coefficient against the bulk-flow Reynolds number, $Re_b = U_b 2h/\nu$, for all simulations. The same plot includes the laminar result and the original correlation proposed by Dean [56], $C_f = 0.073 Re_b^{-0.25}$ for the range $6 \times 10^3 \leqslant Re_b \leqslant 6 \times 10^5$. The DNS result [54] is also shown for reference. The simulation results for $Re_\tau = 2003$, DNS and LES, are seen to be in accord with the proposed correlation. The variance between simulation A2K and the DNS is 0.18%. The cases for $Re_\tau = 20,000$ are beyond the limit of validity of Dean's correlation and there seems to be a tendency upwards with respect to this correlation, if we consider the higher Reynolds number cases. While this behavior is supported by experience in high Reynolds number boundary layers in unconfined flow, there is no experimental evidence for such high Reynolds numbers in channel flow and we refrain from drawing any conclusions as to the predicted behavior of the friction coefficient at high Reynolds numbers for channel flow. Nevertheless, if taken at face value, the resulting inferred wall shear stress represents a prediction.

An important attribute of the wall model employed is the instantaneous dependence of the shear stress on the wall-parallel velocity. This implies a distribution of shear stresses at the wall. The wall-parallel velocity, shear stress, and inner-scaled distance of the first grid next to the wall were extracted to investigate their variability. Fig. 6 shows normalized probability distribution functions of the coordinate of the center of all the first grid cells off-wall in terms of inner variables for all simulations. Essentially, this corresponds to all the values of y_1^+ from Eq. (29). We observe that the PDF of y_1^+ at different Reynolds numbers scales well when normalized with its mean and variance. Moreover, the probability of $y_1^+ < y^* \approx 11$ is extremely small, as the values of $\langle y_1^+ \rangle$ and $\sigma_{y_1^+}$ reported in Table 2 reflect.

Fig. 7 shows histograms of instantaneous streamwise velocity scaled with inner variables and the normalized shear stress at both walls; angle brackets denote wall-parallel averages. Substantial fluctuations are observed in $\tau_{w,1}$, approximately 25% of the mean value, for case A2K. The profiles become narrower as the Reynolds number increases owing to the increased scaled size of the cells and larger mean $\tau_{w,1}$ with increasing Reynolds number. Even though the closure is based on the application of the average Law-of-the-Wall, substantial variability is sustained by the use of this average relationship in an instantaneous manner. Nevertheless, this variability is insufficient to contribute measurable deviations in the statistical results. An *a posteriori*

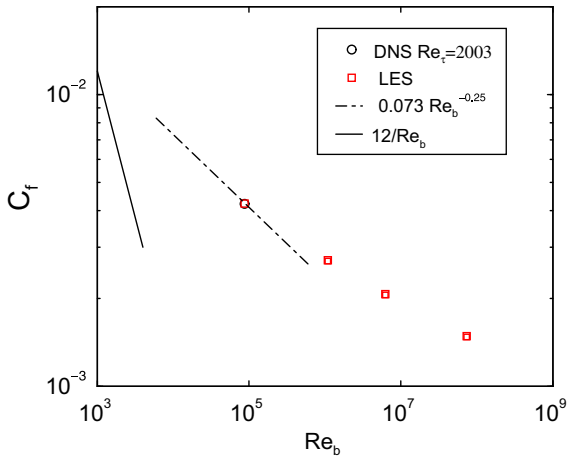

Fig. 5. Predicted and empirical friction coefficient dependence on bulk Reynolds number.

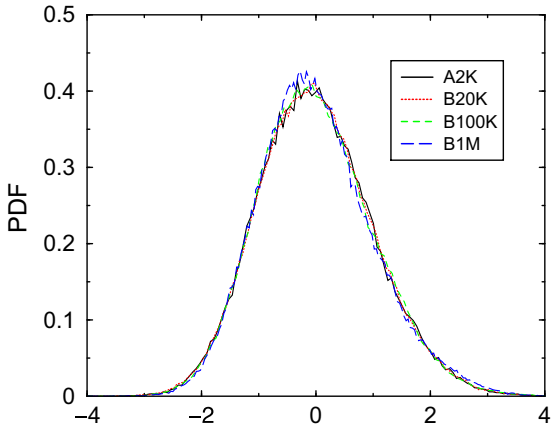

Fig. 6. PDF of the first off-wall grid cell location, y_1^+, normalized in terms of $(y_1^+ - \langle y_1^+ \rangle)/\sigma_{y_1^+}$.

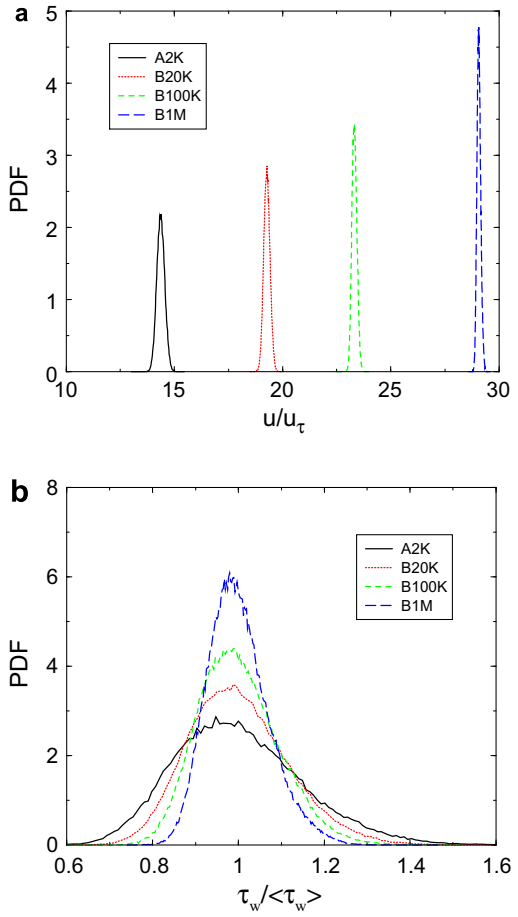

Fig. 7. Histograms of the instantaneous streamwise velocity (a) and shear stress (b) for all cells next to the wall: (a) streamwise velocity in inner scaling; (b) normalized shear stress.

estimate of the differences between using instantaneous values of $\tilde{u}_\alpha$, instead of Eq. (28) with a realistic $\mathcal{P}$ only showed a discrepancy in $\tau_{w,\alpha}$ inferior by 0.4% to the mean value.

Finally, the spatial structure of the streamwise velocity field is also investigated. Fig. 8 shows isocontours of $\tilde{u}$ at three different planes. The streamwise correlation is evident. This is also observed with other methods utilizing wall functions or even more-complicated boundary-layer equation matching. These so-called "super-streaks" are not physical and have sometimes been presented as a cause for concern within the modeling community. In our case, there is substantially more structure to the field, similar to what is observed in methods utilizing stochastic forcing [31], but our results appear less disorganized. This streamwise correlation is completely destroyed by the time the center of the domain is reached and appears to be confined to the region close to the wall. The higher degree of "randomness" in our results may also be associated with the use of the stretched-vortex subgrid model that is known to exhibit rich fine-scale structure. Fig. 9 shows the average one-dimensional spanwise spectra of $\tilde{u}$ for the velocity in the first plane off-wall for all cases. We observe a broad spectral content that we associate with the structural correlation observed in Fig. 8(a).

As the results show, the current closure offers improvements over results previously reported when using the same ingredient, i.e., an instantaneous wall-function model. We do not compare with more involved closures

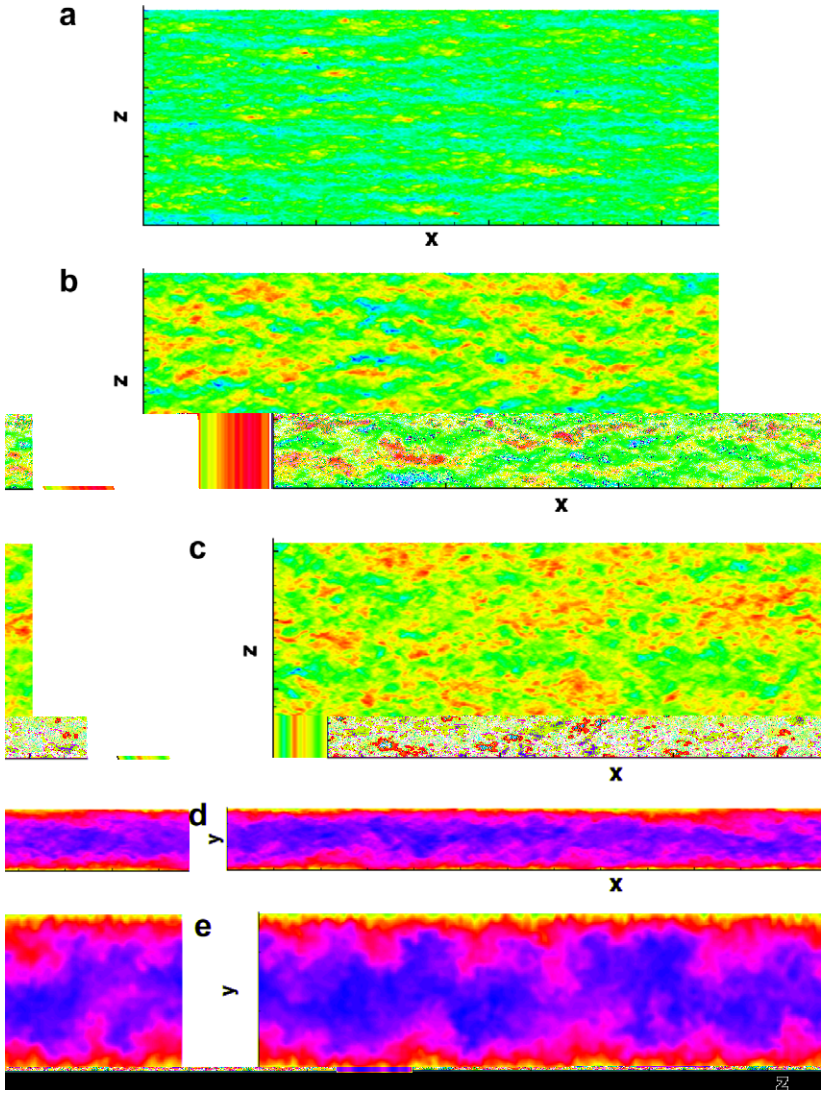

Fig. 8. Isocontours of the streamwise velocity at different planes parallel and perpendicular to the walls for simulation A2K: (a) $y = \Delta y/2$; (b) $y = h/2$; (c) $y = h$; (d) $z = 3\pi h/2$; (e) $x = 0$.

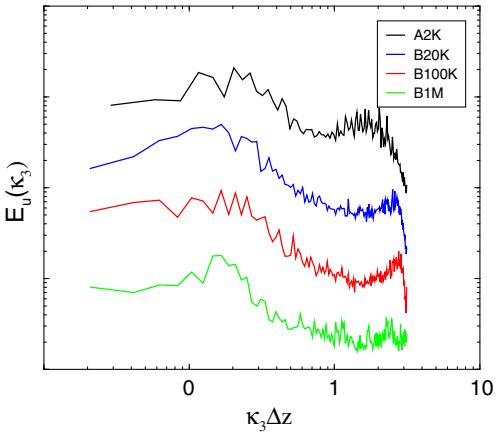

Fig. 9. Spanwise velocity spectra in the spanwise direction at $x_2 = \Delta x_2/2$ for all simulations.

that employ zonal models or even additional transport equations next to the wall, as in detached-eddy simulation, since the comparison is on a different basis (in terms of the amount of information built into the models). Additionally, we do not suspect that the compressible nature of the equations plays any role in the presented simulations. Other simulations at $Re_\tau = 2003$ conducted at both lower and slightly higher Mach numbers (not reported here), while characterized by different execution times, did not exhibit discernible differences in the results reported [6]. We observed that discrete conservation led to improvements in the results, but these were not as good as the results reported here. The final ingredient that improved the results involved the correct extrapolation of the velocity field allowing the subgrid model to predict the subgrid stresses more accurately in the cell wall, at $x_2 = \Delta x_2$.

5. Discussion

The formulation of a wall-function closure for coarse LES, described above, uses the stretched vortex subgrid-scale model and utilizes a combination of elements introduced in the context of shear-stress closures of other subgrid models, as discussed above. Several elements are incorporated simultaneously, such as low numerical dissipation, discrete conservation and boundary condition separation, which seem to result in good results for first-order statistics and acceptable results for second-order statistics. Despite the success, at least two issues deserve further discussion. Firstly, it is expected that correct first-order statistics imply force balance, which is provided by the imposed shear stress closure. Secondly, there is the issue of second-order statistics which are shown in our simulations to drop below their expected values at the first grid cell close to the wall but seem to recover quite rapidly by the fourth-grid cell (counting from the wall). The sharp transition seems to excite a mild amount of Gibbs phenomena that are discernible in our results, perhaps because of the low-numerical dissipation nature of the numerics. Each of these issues are discussed below.

5.1. Shear-stress boundary condition

For the sake of simplicity, we assume that the density is constant in the following discussion, which at the low compressibility level of the flow makes the density effectively constant and uniform throughout the domain. Simulating the outer region of the turbulent channel flow, consist in solving Eq. (1), which for the streamwise momentum component reads,

$$\frac{\partial \rho \tilde{u}}{\partial t} + \frac{\partial \overline{F}_{1,m}}{\partial x_m} = -\frac{\partial P}{\partial x} \tag{47}$$

with a boundary condition, $\overline{F}_{1m} n_m = \tau_w(\tilde{u})$ and $\tilde{v} = 0$ at $y = \pm h$, where $\partial P/\partial x$ is the constant pressure gradient that drives the flow. We have omitted all possible parameters appearing in the shear stress model, τ_w, to

simplify the notation and retained explicitly only the argument that varies in space and time, namely $\tilde{u}$. Integrating across the domain, V, gives

$$\frac{\mathrm{d}(\rho U_\mathrm{b})}{\mathrm{d}t} + \frac{1}{V}\int_W \overline{F}_{1,m} n_m \,\mathrm{d}S = -\frac{\partial P}{\partial x}, \tag{48}$$

where, as before, U_b denotes the volume-averaged velocity and S denotes the surface of the upper and lower walls of the channel. Using the boundary condition, Eq. (12), we can transform the previous expression into

$$\frac{\mathrm{d}(\rho U_\mathrm{b})}{\mathrm{d}t} = -\frac{\partial P}{\partial x} - \frac{\overline{\overline{\tau}}_\mathrm{w}(t)}{h}, \tag{49}$$

where

$$\overline{\overline{\tau}}_\mathrm{w}(t) = \frac{h}{V}\int_W \tau_\mathrm{w}(\tilde{u})\,\mathrm{d}S = \frac{1}{2}\int\int \tau_\mathrm{w}(\tilde{u}(x,-h,z,t)) + \tau_\mathrm{w}(\tilde{u}(x,h,z,t))\,\mathrm{d}x\,\mathrm{d}z. \tag{50}$$

Eq. (49) expresses the integrated conservation of momentum, which is valid instantaneously. There is no large domain, homogeneity, or statistical stationary assumption built in this result.

The question of stability of the boundary conditions, Eq. (12), can be qualitatively investigated if $\overline{\overline{\tau}}_\mathrm{w}(t)$ is expressed in terms of $U_\mathrm{b}(t)$, that is $\overline{\overline{\tau}}_\mathrm{w}(t) = \overline{\overline{\tau}}_\mathrm{w}[U_\mathrm{b}(t)]$. We only require that this change of variables is performed formally, since it may not be practical because the change of variable requires integration of the Navier–Stokes solution and possibly monotonicity of the temporal dependence on time of both $\overline{\overline{\tau}}_\mathrm{w}(t)$ and $U_\mathrm{b}(t)$. This could, in principle, be achieved by increasing the domain size such that statistical variations are averaged out from the integral quantities. Assuming this change of variable is certainly formally possible. Eq. (49) then leads to a stable system if $\mathrm{d}\overline{\overline{\tau}}_\mathrm{w}/\mathrm{d}U_\mathrm{b} > 0$, since the general solution of Eq. (49) is given to second-order in $(U_\mathrm{b}(t) - U_\mathrm{b}^*)$ by

$$\rho U_\mathrm{b}(t) = \rho U_\mathrm{b}^* + \rho(U_\mathrm{b}(0) - U_\mathrm{b}^*)\exp\left(-\frac{\mathrm{d}\overline{\overline{\tau}}_\mathrm{w}}{\mathrm{d}U_\mathrm{b}}(U_\mathrm{b}^*)\frac{t}{\rho h}\right), \tag{51}$$

where U_b^* is the solution to,

$$-\frac{\partial P}{\partial x} - \frac{\overline{\overline{\tau}}_\mathrm{w}(U_\mathrm{b}^*)}{h} = 0. \tag{52}$$

This is generally the case for practical wall-function or shear-stress boundary conditions and it is the expected physical behavior.

Inspection of Eq. (49) indicates that the pressure gradient is in statistical balance (the time-rate-of-change of the bulk velocity averages to zero in a sufficiently large time interval) with the shear stress at the wall, *independently* of the functional form of $\tau_\mathrm{w}(\tilde{u})$. This is just a consequence of Eq. (50). Integrating the governing equations with boundary conditions, Eq. (12), produces a velocity at the wall as required to keep Eq. (49) in statistical balance with the pressure. This comes at a cost, resulting in a wall velocity, $\tilde{u}(x,\pm h,z,t)$, that need not to agree with the experimentally expected logarithmic law of the wall. This implies that any mismatch between the expected shear stress dependence on the velocity, whether from modeling error or numerics, will result in a wall velocity which is inconsistent with the required result, as dictated by the conservation of momentum. The difference will be such that Eq. (50) integrates to statistically balance the pressure gradient at the cost of the value of $\tilde{u}$ at the wall. The discretely conserving formulation employed implies that Eq. (50) is enforced discretely.

5.2. Inner–outer matching

A second aspect of an outer region simulation is associated with the boundary condition for the wall-normal velocity. Conservation of mass requires that $\tilde{v}$ vanish at the wall. This condition could be relaxed by requiring that $\tilde{v}$ possesses a statistical variation with zero mean. The main concern, expressed in the Schumann [3] formulation, is that the vertical velocity is not identically zero at the location where the inner–outer matching is performed, $y^+ > 30$. At this location, the vertical velocity fluctuations can be of the order of half those of

the streamwise component (a ratio that depends in general on the Reynolds number and the matching location). Therefore, a boundary condition for the wall normal velocity could be imposed that has zero mean and a specified variance. Unfortunately, once one decides to follow this path, correlations with the wall-parallel velocities must be taken into account. Moreover, such statistical velocity boundary conditions require a certain degree of spatial and temporal smoothness for the numerical method to behave adequately. A white noise stochastic signal leads to excessive dissipation and noise pollution at the boundary and cannot be used. It is possible to construct a random signal with imposed one- and two-point spatial and temporal statistics and which could be made physically reasonable. The main drawback is that, in order to preserve the statistical properties of the signal, the boundary condition becomes non-local since the boundary condition of the whole wall surface must be generated. We did attempt this technique and observed in short runs that the drop of the second-order velocity statistics at the first grid cell and small amount of Gibbs phenomena disappeared. Unfortunately, the formulation was not found to be stable in very long runs and further research is required.

We close the discussion by noting that the generality of the approach discussed relies, of course, on the validity of the particular inner–outer matching condition. As noted above, the Law-of-the-Wall parameterization employed is appropriate for the smooth-wall, near-zero pressure-gradient case at hand. Other smooth-wall parameterizations, such as the one proposed by Nickels [43] could be used to extend the validity of the approach to favorable as well as unfavorable pressure gradient turbulent boundary layer wall conditions, with the latter just short of boundary-layer separation. Of course, separation presents a challenge of a different kind since, in the separation region, where $\partial p/\partial y$ cannot be ignored, the boundary-layer approximation itself breaks down and a structural extension of the approach proposed here is required. Once the boundary layer separates, forming a local free-shear layer, the proposed scheme is able to handle the local dynamics, with modeling of the reattachment region also posing a challenge. This phenomenology poses challenges that must eventually be addressed but are beyond the scope of this paper. A second issue briefly discussed above is the issue of wall roughness, in particular, at spatial scales below those resolved by the LES. At least in the absence of significant pressure gradients, well-established parameterizations exist to accommodate (unresolved) wall roughness. While we do not consider this as presenting a fundamental challenge, it too is beyond the scope of the present discussion. The combination of wall-roughness and imposed pressure-gradient effects is a topic of current research and a numerical simulation based on the methodology documented above must await the results of such research.

6. Conclusions

We present a numerical and physical subgrid closure for simulating the outer scales of turbulent wall-bounded flows using large-eddy simulation. Good predictions of important low-order statistics of the outer-region of turbulent channel flow are documented. The method requires the use of a wall-function closure formulated directly on the conservatively discretized momentum equations. We show that the presence of the wall requires special attention to the details of how the subgrid model is evaluated next to the wall. This is achieved by constructing a surrogate velocity field used by the subgrid-scale model that consists of an extrapolation of the velocity field within the computational domain. Finally, the stretched-vortex model is used away from walls. In this treatment, one recovers reasonably good first- and second-order statistics with isotropic and uniform mesh spacing. The use of empirical damping functions is not required. Only the (logarithmic) Law-of-the-Wall is used. Test simulations for Reynolds numbers up to $Re_\tau = 10^6$ yield reasonable results. This includes predictions of the friction coefficient, where good agreement with an empirical correlation is observed.

Investigation of the spatial correlation of the instantaneous streamwise velocity field next to the wall shows fine structure, like that observed in more complex models that also inject statistical fluctuations (randomness) as part of the boundary condition. This is obtained at no additional modeling cost.

Acknowledgments

We acknowledge fruitful discussions with Dr. A. Ferrante and thank the reviewers for many valuable comments. This work was largely undertaken while the first author resided at the California Institute of Technol-

ogy, and was supported by AFOSR Grants FA9550-04-1-0020 and FA9550-04-1-0389, and by the Advanced Simulation and Computing (ASC) Program under Subcontract No. B341492 of the DOE Contract W-7405-ENG-48.

References

[1] P.J. Mason, Large-eddy simulation – a critical-review of the technique, Quart. J. Roy. Meteorol. Soc. 120 (515) (1994) 1–26.
[2] S.B. Pope, Ten questions concerning the large-eddy simulation of turbulent flows, New J. Phys. 6 (35) (2004).
[3] U. Schumann, Subgrid scale model for finite difference simulations of turbulent flows in plane channels and annuli, J. Comput. Phys. 18 (1975) 376–404.
[4] J.S. Baggett, J. Jiménez, A.G. Kravchenko, Resolution requirements in large-eddy simulations of shear flows, Annual research briefs, Center for Turbulence Research, Stanford University, 1997, pp. 51–66.
[5] A. Pascarelli, U. Piomelli, G.V. Candler, Multi-block large-eddy simulations of turbulent boundary layers, J. Comput. Phys. 157 (1) (2000) 256–279.
[6] H. Foysi, S. Sarkar, R. Friedrich, Compressibility effects and turbulence scalings in supersonic channel flow, J. Fluid Mech. 509 (2004) 207–216.
[7] H. Schlichting, Boundary-Layer Theory, McGraw-Hill, 1955.
[8] U. Piomelli, E. Balaras, Wall-layer models for large-eddy simulations, Annu. Rev. Fluid Mech. 34 (2002) 349–374.
[9] U. Piomelli, P. Moin, J.H. Ferziger, Model consistency in large eddy simulation of turbulent channel flows, Phys. Fluids 31 (7) (1988) 1884–1891.
[10] L. Temmerman, M.A. Leschziner, C.P. Mellen, J. Frohlich, Investigation of wall-function approximations and subgrid-scale models in large eddy simulation of separated flow in a channel with streamwise periodic constrictions, Int. J. Heat Fluid Flow 24 (2) (2003) 157–180.
[11] W. Cabot, P. Moin, Approximate wall boundary conditions in the large-eddy simulation of high Reynolds number flow, Flow Turbul. Combust. 63 (1–4) (2000) 269–291.
[12] J.W. Deardorff, A numerical study of three-dimensional turbulent channel flow at large Reynolds numbers, J. Fluid Mech. 41 (1970) 453–480.
[13] C.H. Moeng, A large-eddy-simulation model for the study of planetary boundary-layer turbulence, J. Atmos. Sci. 41 (13) (1984) 2052–2062.
[14] P.J. Mason, N.S. Callen, On the magnitude of the subgrid-scale eddy coefficient in large-eddy simulations of turbulent channel flow, J. Fluid Mech. 162 (1986) 439–462.
[15] G.Grötzbach, Grötzbach, Direct numerical and large eddy simulation of turbulent channel flows, in: N.P. Cheremisinoff (Ed.), Encyclopedia of Fluid Mechanics, Gulf, West Orange, NJ, 1987.
[16] U. Piomelli, J. Ferziger, P. Moin, J. Kim, New approximate boundary conditions for large eddy simulation of wall-bounded flows, Phys. Fluids A 1 (6) (1989) 1061–1068.
[17] G. Hoffmann, C. Benocci, Approximate wall boundary conditions for large-eddy simulations, in: R. Benzi (Ed.), Advances in Turbulence V, Kluwer, Berlin, 1995.
[18] F. Nicoud, J.S. Baggett, P. Moin, W. Cabot, Large eddy simulation wall-modeling based on suboptimal control theory and linear stochastic estimation, Phys. Fluids 13 (10) (2001) 2968–2984.
[19] P. Quemere, P. Sagaut, Zonal multi-domain RANS/LES simulations of turbulent flows, Int. J. Numer. Methods Fluids 40 (7) (2002) 903–925.
[20] J.A. Templeton, G. Medic, G. Kalitzin, An eddy-viscosity based near-wall treatment for coarse grid large-eddy simulation, Phys. Fluids 17 (10) (2005) 105101.
[21] M. Abel, D. Stojkovic, M. Breuer, Nonlinear stochastic estimation of wall models for LES, Int. J. Heat Fluid Flow 27 (2) (2006) 267–278.
[22] E. Balaras, C. Benocci, Subgrid-scale models in finite-difference simulations of complex wall bounded flows, Technical Report, AGARD CP 551, Neuilly-Sur-Seine, 1994, pp. 2.1–2.5.
[23] W. Cabot, Large-eddy simulations with wall models, Annual research briefs, Center for Turbulence Research, Stanford University, 1995, pp. 41–50.
[24] E. Balaras, C. Benocci, U. Piomelli, Two-layer approximate boundary conditions for large-eddy simulations, AIAA J. 34 (6) (1996) 1111–1119.
[25] P.R. Spalart, W.-H. Jou, M. Strelets, S.R. Allmaras, Comments on the feasibility of LES for wings, and on hybrid RANS/LES approach, in: C. Liu, Z. Liu (Eds.), Advances in DNS/LES, Greyden, Columbus, OH, 1997.
[26] E.Y.K. Ng, H.Y. Tan, H.N. Lim, D. Choi, Near-wall function for turbulence closure models, Comput. Mech. 29 (2002) 178–181.
[27] N. Nikitin, F. Nicoud, B. Wasistho, K.D. Squires, P. Spalart, An approach to wall modeling in large-eddy simulations, Phys. Fluids 12 (2000) 1629.
[28] F. Porté-Agel, C. Meneveau, M.B. Parlange, A scale-dependent dynamic model for large-eddy simulation: application to a neutral atmospheric boundary layer, J. Fluid Mech. 415 (2000) 261–284.
[29] R.C. Schmidt, A.R. Kerstein, S. Wunsch, V. Nielsen, Near-wall LES closure based on one-dimensional turbulence modeling, J. Comput. Phys. 186 (1) (2003) 317–355.

[30] U. Piomelli, E. Balaras, H. Pasinato, K.D. Squires, P.R. Spalart, The inner–outer layer interface in large-eddy simulations with wall-layer models, Int. J. Heat Fluid Flow 24 (4) (2003) 538–550.
[31] A. Keating, U. Piomelli, A dynamic stochastic forcing method as a wall-layer model for large-eddy simulation, J. Turbul. 7 (12) (2006) 1–24.
[32] P.P. Sullivan, J.C. McWilliams, C.H. Moeng, A subgrid-scale model for large-eddy simulation of planetary boundary-layer flows, Bound.-Lay. Meteorol. 71 (3) (1994) 247–276.
[33] B. Kosovic, Subgrid-scale modelling for the large-eddy simulation of high-Reynolds-number boundary layers, J. Fluid Mech. 336 (1997) 151–182.
[34] P.J. Mason, D.J. Thomson, Stochastic backscatter in large-eddy simulations of boundary-layers, J. Fluid Mech. 242 (1992) 51–78.
[35] A. Misra, D.I. Pullin, A vortex-based subgrid stress model for large-eddy simulation, Phys. Fluids 9 (1997) 2443–2454.
[36] B. Kosovic, D.I. Pullin, R. Samtaney, Subgrid-scale modeling for large-eddy simulations of compressible turbulence, Phys. Fluids 14 (2002) 1511–1522.
[37] T.S. Lundgren, Strained spiral vortex model for turbulent fine-structure, Phys. Fluids 25 (1982) 2193–2203.
[38] T. Voelkl, D.I. Pullin, D.C. Chan, A physical-space version of the stretched-vortex subgrid-stress model for large-eddy simulation, Phys. Fluids 12 (2000) 1810–1825.
[39] M. Lesieur, O. Metais, New trends in large-eddy simulations of turbulence, Annu. Rev. Fluid Mech. 28 (1996) 45–82.
[40] D.I. Pullin, A vortex-based model for the subgrid flux of a passive scalar, Phys. Fluids 12 (2000) 2311–2319.
[41] E.S. Zanoun, F. Durst, H. Nagib, Evaluating the law of the wall in two-dimensional fully developed turbulent channel flows, Phys. Fluids 15 (10) (2003) 3079–3089.
[42] W.K. George, Recent advancements toward the understanding of turbulent boundary layers, AIAA J. 44 (11) (2006) 2435–2449.
[43] T.B. Nickels, Inner scaling for wall-bounded flows subject to large pressure gradients, J. Fluid Mech. 521 (2004) 217–239.
[44] M. Iovieno, G. Passoni, D. Tordella, A new large-eddy simulation near-wall treatment, Phys. Fluids 16 (11) (2004) 3935–3944.
[45] C. Pantano, R. Deiterding, D.J. Hill, D.I. Pullin, A low numerical dissipation patch-based adaptive mesh refinement method for large-eddy simulation of compressible flows, J. Comput. Phys. 221 (1) (2006) 63–87.
[46] S. Ghosal, An analysis of numerical errors in large-eddy simulations of turbulence, J. Comput. Phys. 125 (1) (1996) 187–206.
[47] D.J. Hill, D.I. Pullin, Hybrid tuned center-difference-WENO method for large eddy simulations in the presence of strong shocks, J. Comput. Phys. 194 (2) (2004) 435–450.
[48] Y. Benarafa, O. Cioni, F. Ducros, P. Sagaut, RANS/LES coupling for unsteady turbulent flow simulation at high Reynolds number on coarse meshes, Comput. Methods Appl. Mech. Eng. 195 (23–24) (2006) 2939–2960.
[49] M. Popovac, K. Hanjalic, Compound wall treatment for RANS computation of complex turbulent flows and heat transfer, Flow Turbul. Combust. 78 (2007) 177–202.
[50] P.M. Gresho, R.L. Sani, Incompressible Flow and the Finite Element Method, Wiley, 2000.
[51] R. Courant, D. Hilbert, Methods of Mathematical Physics, vol. 2, Wiley, 1991.
[52] A. Andrén, A.R. Brown, J. Graf, P.J. Mason, C.-H. Moeng, F.T.M. Nieuwstadt, U. Schumann, Large-eddy simulation of the neutrally stratified boundary layer: a comparison of four computer codes, Quart. J. Roy. Meteorol. Soc. 120 (1994) 1457–1484.
[53] E. Balaras, C. Benocci, U. Piomelli, Finite-difference computations of high Reynolds-number flows using the dynamic subgrid-scale model, Theor. Comput. Fluid Dyn. 7 (3) (1995) 207–216.
[54] S. Hoyas, J. Jiménez, Scaling of the velocity fluctuations in turbulent channels up to $Re = 2003$, Phys. Fluids 18 (1) (2006) 011702.
[55] D. Coles, The law of the wake in the turbulent boundary layer, J. Fluid Mech. 1 (1956) 191–226.
[56] R.B. Dean, Reynolds number dependence of skin friction and other bulk flow variables in two-dimensional rectangular duct flow, J. Fluids Eng. Trans. ASME 100 (2) (1978) 215–223.